Article

Pavement Performance Investigation of Nano-TiO₂/CaCO₃ and Basalt Fiber Composite Modified Asphalt Mixture under Freeze-Thaw Cycles

Yafeng Gong, Haipeng Bi, Zhenhong Tian and Guojin Tan *

College of Transportation, Jilin University, Changchun 130022, China; gongyf@jlu.edu.cn (Y.G.);
bihp@jlu.edu.cn (H.B.); Tianzh@jlu.edu.cn (Z.T.)
* Correspondence: Tgj@jlu.edu.cn; Tel.: +86-155-2688-5763

check for updates

Abstract: The objective of this research is to evaluate the pavement performance degradation of nano-TiO₂/CaCO₃ and basalt fiber composite modified asphalt mixtures under freeze-thaw cycles. The freeze-thaw resistance of composite modified asphalt mixture was studied by measuring the mesoscopic void volume, stability, indirect tensile stiffness modulus, splitting strength, uniaxial compression static, and dynamic creep rate. The equal-pitch gray prediction model GM (1, 3) was also established to predict the pavement performance of the asphalt mixture. It was concluded that the high- and low-temperature performance and water stability of nano-TiO₂/CaCO₃ and basalt fiber composite modified asphalt mixture were better than those of an ordinary asphalt mixture before and after freeze-thaw cycles. The test results of uniaxial compressive static and dynamic creep after freeze-thaw cycles showed that the high-temperature stability of the nano-TiO₂/CaCO₃ and basalt fiber composite modified asphalt mixture after freeze-thaw was obviously improved compared with an ordinary asphalt mixture.

Keywords: nanometer materials; basalt fiber; composite modified asphalt mixture; freeze-thaw cycle; damage model

1. Introduction

Due to the good performance and riding quality, along with easy maintenance and repair, asphalt pavement has increased year by year in China [1]. However, the temperature sensitivity of asphalt materials is high and the mechanical properties of asphalt pavement will degrade under large temperature difference [2]. Northeast China belongs to the seasonal frozen region and the average temperature in winter can reach −20 °C and above 20 °C in summer. In order to improve the performance of asphalt pavement, reduce the damage of pavement, and extend the service life of pavement, nanomodification and fiber modification technologies have been applied in asphalt mixture.

Nanotechnology is a new technology that has gradually emerged in recent years. Nanomaterials have been gradually applied as asphalt mixture modifiers due to their special properties not found in macroscopic materials. Ameri et al. evaluated moisture susceptibility of hot mix asphalt (HMA) with and without Zycosoil as a nano-organosilane anti-stripping additive and hydrated lime in the form of slurry. The results found that use of Zycosoil additive will increase adhesion bond between the aggregates and asphalt binders, and in turn influences the moisture resistance of the mixture to moisture damage [3]. Hamedi studied the effects of using nano-CaCO₃ as an antistrip additive on moisture susceptibility of asphalt mixtures have been assessed using the surface free energy (SFE) method and modified Lottman test. Adding nanomaterials lead to the decrease of the acid component of SFE and increase of basic component of SFE for the asphalt binder that lead to an increase of

adhesion between the asphalt binder and sensitive aggregate against moisture damage [4]. Nano-TiO_2 is a commonly used nanomodified material. Shafabakhsh et al. found that nano-TiO_2 could effectively improve the viscosity, anti-rutting, and anti-fatigue properties of asphalt mixture [5]. Sadeghnejad et al. used nanomaterials to modify SMA and the test results showed that nano-TiO_2 could improve the anti-rutting ability and splitting strength ratio and prolong the service life of an asphalt mixture [6]. Nazari et al. evaluated the microstructure and chemical properties of nanocomposite modified asphalt by X-ray and scanning electron microscopy. It was found that the addition of nanomaterials improved the fatigue resistance of asphalt mixture [7].

There are many kinds of fiber modifiers used in asphalt mixtures in recent years, such as polyester fiber, lignin fiber, carbon fiber, glass fiber, basalt fiber, etc. Different fiber modifiers have their own advantages and disadvantages. The low-temperature crack resistance of asphalt mixture is the main problem in the frozen region of northeast China. Compared with other fibers, basalt fiber is a mineral fiber that is abundant and easy to obtain in northeast China. Also, it will not cause environmental pollution. Basalt fiber has some advantages in terms of modifying road performance of asphalt mixtures. Zheng studied the pavement performances of basalt fiber, lignin fiber, and polyester fiber modified asphalt mixtures and found that the performance of the basalt fiber modified asphalt mixture was superior to that of the others [8,9]. Morova et al. studied the usability of basalt fibers in order to bear the stresses occurring at the surface layer of pavement and the optimum value of the fiber ratio leading to the optimum stability value was determined [10]. Chen found that basalt fiber, at the optimal fiber content, could improve the water stability and high-temperature stability of the asphalt mixture more effectively than lignin fiber and polyester fiber [11]. Qin studied the asphalt adsorption property, shear performance, crack resistance, and high-temperature rheological properties of asphalt modified by basalt fiber, lignin fiber, and polyester fiber. The microstructure and strengthening mechanism of basalt fiber was also studied by scanning electron microscopy. The results showed the basalt fiber can obviously improve the crack resistance of asphalt mastic than other fibers [12]. Gao et al. found that basalt fiber could significantly improve the tensile strength of asphalt mixture [13]. Chang et al. studied the low-temperature performance of asphalt mixture under salt freeze-thaw cycles with low-temperature bending experiments. The results showed that the concentration of the salt solution and freeze-thaw temperature had significant influence on the low-temperature performance of mixture. Basalt fiber improved the low-temperature performance of mixture under salt freeze-thaw cycles [14]. Davar et al. evaluated the fatigue life of basalt fiber and diatomite composite modified asphalt with four-point bending beam experiment, and the experimental results showed that basalt fiber improved the low-temperature performance of asphalt mixture [15]. Zheng et al. studied the performance of basalt modified asphalt mixture under the coupling effect of chloride erosion and freeze-thaw cycles. It was found that basalt fiber greatly improved the low-temperature bending and fatigue performances of asphalt mixture [16]. In addition, basalt fiber could improve the resistance and pavement performance of asphalt road under complex environment. Zhang et al. studied the performance improvement of asphalt mixtures modified with different modifiers at different salt concentrations and different environments. The test results showed that basalt fiber had the best improvement on mechanical properties of asphalt mixtures under salty and humid environment [17,18]. Celauro et al. studied the performances of basalt fiber modified asphalt mixture as the surface layer of bus lane pavement, and found that basalt fiber modified asphalt had good performance in resisting permanent deformation and increasing road friction [19]. The raw material cost of basalt fiber modified asphalt pavement has increased by 15–20%, but the service life of the pavement can increase by 30–40% [20,21]. From what has been discussed above, basalt fiber is suitable to be used as a modified material for asphalt pavement in northeast China.

The asphalt concrete pavement in northeast China faces the freeze–thaw cycles conditions. The freeze-thaw cycles had a great threat to the durability of asphalt pavement. Many researchers analyzed the mechanism of freeze-thaw damage of asphalt mixture, in general, the water permeated and remained in the pores of the pavement, when the external temperature decreased, the pore water

froze and volume expanded, which resulted in the generation of frost heave. When the temperature increased, ice melted into water and began the next freeze-thaw cycle. With repeated freeze-thaw cycle, the internal pore morphology and bituminous viscosity of the mixture were significantly changed and the performances of the mixture were significantly reduced [22–25]. In order to more vividly reflect the mechanism of freeze-thaw damage of asphalt mixture, research focused on the performance changes of asphalt mixture under freeze-thaw cycles through macroscopic test or mesoscopic analysis. Xu et al. studied the micro-thermodynamic behavior of asphalt mixtures under a freeze-thaw cycle with information entropy theory, X-ray tomography and image processing technology [26]. Nian performed the freeze-thaw aging test and carried out Fourier transform infrared spectroscopy quantitative to analyze the compositions and rheological properties of asphalt mixture in cold regions [27]. Xu et al. studied the internal evolution and analyzed the pore distribution changes and permeability of asphalt mixture during a freeze-thaw cycle with X-ray tomography [28,29]. Wang et al. analyzed the pore structure of semi-rigid base materials under freeze-thaw cycles with X-ray tomography [30]. Ma et al. established the performance decay model of asphalt pavement in cold regions. The results showed that the freeze-thaw cycles had a significant impact on pavement reliability. The more unstable the conditions of the freeze-thaw cycle, the greater the impact on pavement capacity [31]. Sol-Sánchez analyzed the evolution of the strength and bearing capacity of asphalt mixtures exposed to long-term moisture over several freeze-thaw cycles and a varying number of days of thermal aging. It found that the air void content has a significant influence on the long-term evolution of the mixture properties under moisture, which is a reversible process, unlike the other two climate agents studied [32]. Badeli et al. studied the changes of complex modulus of asphalt mixtures under rapid freeze-thaw cycles with different compaction and dry humidity in cold regions. They established rheological model to predict the service life and fatigue crack of asphalt mixture under freeze-thaw cycles. It was found that the freeze-thaw cycles had a more significant effect on the stiffness of the mixture [33–35]. Gong et al. studied the effect of freeze-thaw cycles on mortar with the rheological test of curved beam [36]. Linares used three representation functions to determine relaxation moduli of asphalt mixtures subject to the action of freeze-thaw cycles. It concludes that Prony series function appeared to have better prediction than other two functions in fitting raw creep compliance data of asphalt mixtures at 0, 100, 200, 250, and 300 freeze-thaw cycles as well as showing promising results in predicting the relaxation modulus of asphalt mixtures subjected to freeze-thaw cycles [37]. Lachance-Tremblay et al. used the 2S2P1D rheological model to simulate the material behavior and evaluate the evolution of linear viscoelastic properties. Repeated freeze-thaw damaged the sample and glass asphalt mixture was damaged faster than the reference mixture. However, both mixtures reached equivalent damage after 10 freeze-thaw cycles [38]. In order to improve the freeze-thaw resistance asphalt pavement, the addition of modified materials was the main methods in existing researches. Huang et al. studied the moisture resistance of asphalt mixture modified with slaked lime under freeze-thaw cycles [39]. Wei et al. studied the influence of diatomite and styrene-butadience-styrence (SBS) on the freeze-thaw resistance of waste rubber modified asphalt mixture. They established the mathematical model and accurately predicted the porosity and indirect tensile strength during freeze-thaw cycles [40]. Modarres et al. studied the effect of Cement kiln dust (CKD) as a filler material on the low-temperature characteristics of hot mix asphalt (HMA). According to the obtained results, mixes containing CKD filler demonstrated better resistance against freeze-thaw cycles compared to the control mixture containing limestone (LS). Moreover, mixes containing CKD exhibited a higher fatigue life compared to the control mix and for all mixes the fatigue life decreased by decreasing the temperature [41]. Yan et al. studied the effects of freeze-thaw cycles on the Marshall stability, flow value, and split tensile strength of stone mastic asphalt (SMA) mixtures with different lime content [42]. Xu et al. studied the effect of freeze-thaw cycles on split tensile strength and porosity of rubber modified asphalt mixture [43]. Teguedi et al. analyzed the local volume change of asphalt mixture with different reclaimed asphalt pavement (RAP) contents under freeze-thaw cycles with grid method and digital image processing technology [44].

In this paper, in order to evaluate whether the freeze-thaw performance of nano-TiO_2/$CaCO_3$ and basalt fiber composite modified asphalt mixture meets the climate requirements of seasonal frozen area, various physical and mechanical properties under freeze-thaw cycles were studied. Two kinds of asphalt mixtures, matrix asphalt mixture (AM) and nano-TiO_2/$CaCO_3$ and basalt fiber composite modified asphalt mixture (NBAM), were prepared with the best oil-stone ratio. The freeze-thaw cycles test was carried out. The degradation and damage mechanism of physical and mechanical properties for different asphalt mixtures were analyzed. The improvements on mechanical properties of nano-TiO_2/$CaCO_3$ and basalt fiber composite modified asphalt mixture after freeze-thaw cycle were studied.

2. Materials and Methods

2.1. Materials

In this paper, base bitumen AH-90 was used as the binder. According to the Chinese national standard (JTGE40-2004) [45], AH-90 is bitumen with penetration between 80 and 100. The penetration, softening point, ductility, Brookfield viscosity and density of bitumen were determined according to the Standard Test Methods of Bitumen and Bituminous Mixtures for Highway Engineering (JTG E20-2011) [46]. The physical indexes of the base bitumen are listed in Table 1.

Table 1. Basic properties of bitumen.

Property	Test Results	Standard Requirements
Penetration (25 °C, 5 s, 0.1 mm)	85.8	80–100
Softening point $T_{R\&B}$ (°C)	46.9	$\geq$45
Ductility (25 °C, cm)	>150	$\geq$100
Brookfield viscosity (135 °C, Pa·s)	306.9	—
Density (15 °C, g/cm^3)	1.016	—

The basalt fiber was used in this paper to modified asphalt mixture. The appearance is shown in Figure 1. The basic technical properties are listed in Table 2. From previous study of our research group on basalt fiber modified asphalt mixture [47], the basalt fiber also has the low hydrophilicity, high heat resistance and high oil absorption (oil absorption rate is 6.154%). Basalt fiber provides a feasibility for the application of composite modified asphalt.
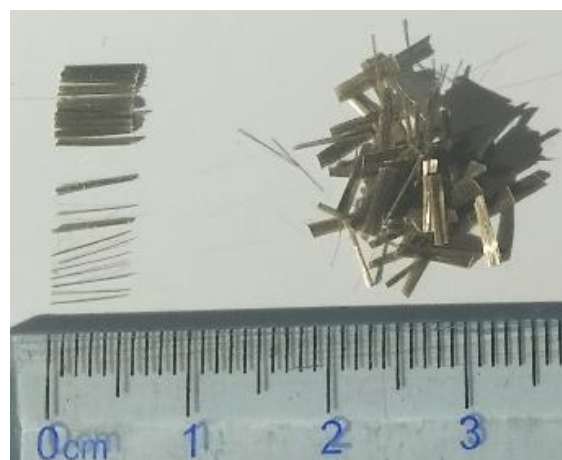

Figure 1. Appearance of basalt fiber.

Table 2. Technical properties of basalt fiber.

Property	Test Results	Standard Requirements [48]
Diameter (μm)	10–13	—
Length (mm)	6	—
Moisture content (%)	0.030	≤ 0.2
Combustible content (%)	0.56	—
Linear density (Tex)	2398	2400 ± 120
Fracture strength (N/Tex)	0.55	≥ 0.40
Tensile strength (MPa)	2320	≥ 2000
Tensile modulus of elasticity (GPa)	86.3	≥ 85
Elongation at break (%)	2.84	≥ 2.5

Nano-materials are white color, made by chemical methods and inorganic synthetic materials. The molecular formula is $TiO_2/CaCO_3$, and the appearance is shown in Figure 2. It is soluble in water. The supporting particles are rod-shaped and the outer titanium dioxide particles are flake-shaped (diameter is 50–60 nm), with regular structure and excellent covering power.

(**a**) (**b**)
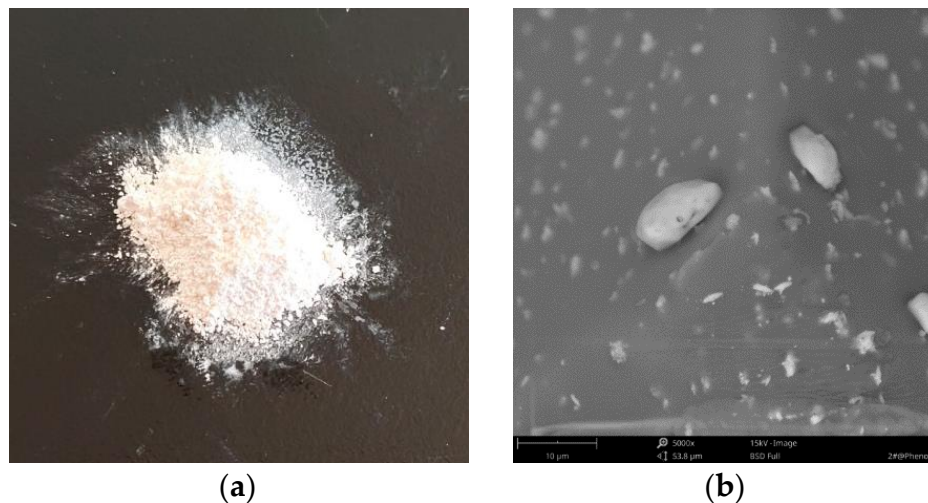
Figure 2. Images of nano $TiO_2/CaCO_3$ materials: (**a**) appearance; (**b**) SEM images (5000×).

The coarse and fine aggregates used in the test were sieved, and the physical properties of coarse aggregates, fine aggregates and mineral powders were tested according to the requirements of JTG E42-2005 [49]. The results are shown in Tables 3–5.

Table 3. Physical properties of aggregate.

Granular Grade (mm)	Apparent Specific Gravity	Saturated Surface—Dry Bulk Specific Gravity	Bulk Specific Gravity	Water Absorption Rate (%)
13.2	3.142	3.066	3.031	1.17
9.5	2.992	2.943	2.917	0.86
4.75	3.084	3.001	2.961	1.35
2.36	2.721	2.646	2.603	1.67
1.18	2.661	2.602	2.566	1.38
0.6	2.758	2.709	2.681	1.07
0.3	2.684	2.635	2.606	1.13
0.15	2.907	2.82	2.776	2.14
0.075	2.627	2.528	2.476	2.04

Table 4. Physical properties of mineral powder.

Project	Unit	Test Results	Specification Requirements (Highway Surface Layer)
Apparent specific gravity	g/cm^3	2.719	≥ 2.5
Moisture content	%	0.19	≤ 1
Particle size < 0.6 mm	%	100	100
Particle size < 0.15	%	95.1	90–100
Particle size < 0.075	%	87.8	75–100
Exterior	—	No agglomeration	No agglomeration
Hydrophilic coefficient	—	0.68	<1

Table 5. Crushed value and wearing values of coarse aggregate.

Technical Indicators (%)	Test Results	Specification Limitation
Crushed value	13.5	≤ 28
Wearing value	16.0	≤ 30

2.2. Preparation of Test Pieces

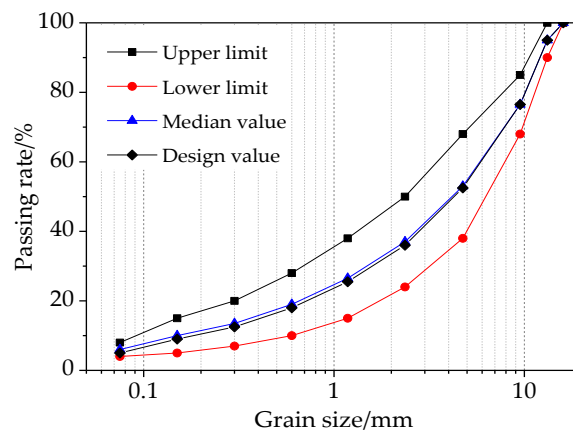The asphalt mixture gradation in this study is AC-13, which is shown in Figure 3.

Figure 3. AC-13 mineral gradation curve.

In this study, the nano-TiO$_2$/CaCO$_3$ and basalt fiber composite modified asphalt was prepared with high-speed shearing method and then the asphalt mixtures were produced. When preparing the modified asphalt, the temperature was 150 °C and the shear rate is 4000 r/min. The asphalt mixtures were prepared according to JTG E20-2011 [46]. The mixing temperature was 160 °C and the double-sided compaction was 75 times. The Marshall specimens in this study were prepared with height of 63.5 $\pm$ 1.3 mm and diameter of 101.6 $\pm$ 0.2 mm. The parameters of asphalt mixture (AM) and nano-TiO$_2$/CaCO$_3$ and basalt fiber composite modified asphalt mixture (NBAM) are shown in Table 6. All specimens were put into the freeze-thaw condition as 0, 5, 10, 15 cycles and after that the properties of two kinds of asphalt mixtures were tested as experimental procedures. The degradation law of the NBAM can be analyzed.

Table 6. Preparation parameter of asphalt mixture specimens.

Group	Basalt Fiber (%)	Nano-Modifier (%)	Asphalt-Aggregate Ratio
AM	0	0	5.00
NBAM	3.9	5.1	5.67

2.3. Freeze-Thaw Cycles Conditions

Considering the climatic conditions in northeastern China, the freeze-thaw cycle test procedure of asphalt mixture specimen is as follows: (a) saturated under vacuum for 30 min; (b) frozen for 16 ± 1 h at $-20\,^{\circ}$C in refrigerator; (c) thawed for 24 h with $60\,^{\circ}$C $\pm 1\,^{\circ}$C water. In order to eliminate the influence of internal pore water on the test results, before each performance test, the specimens were kept in the room at temperature $20 \pm 2\,^{\circ}$C, humidity $40 \pm 5\%$ for two days to ensure that the specimen is as dry as possible.

2.4. Experimental Procedures

2.4.1. Mesoscopic Void Ratio Test

The volume and the open-closed pores morphology were changed under freeze-thaw cycles. It was different to determine the volume of connected pores accurately with the method that measured the mass of specimen submerged in water. Therefore, Computed Tomography (CT) mesoscopic scanning was used to obtain experimental data of mesoscopic void fraction after freeze-thaw. The Brilliancei CT (128 rows and 256 layers) produced by Philips (Amsterdam, The Netherlands) was used and horizontal scanning method was adopted. The testing equipment is shown in Figure 4. The scanning thickness was 0.67 mm and the scanning layer obtained from each specimen was about 100. The scanning temperature was set to 20 °C. The specimens of group AM and NBAM were scanned for CT sections after 0, 5, 10, and 15 freeze-thaw cycles. The image processing software configured by Brilliancei CT was used to obtain scanning images. Then the mesoscopic void ratio can be obtained with image processing technology.

Figure 4. Testing equipment.

2.4.2. Stability Test

The stability test was conducted according to JTG E20-2011 [46], which can be used to reflect the high-temperature performance of asphalt mixtures. The loading rate is 50 mm/min. The specimens after freeze-thaw cycles were treated in the water bath of 60 °C for 30-40 min and then the residual stability was measured. The variation of stability before and after freeze-thaw could be used to characterize the degradation of high-temperature stability under freeze-thaw cycles.

2.4.3. Indirect Tensile Stiffness Modulus Test

The indirect tensile stiffness modulus test (ITSM) was conducted according to AASHTO TP-31 [50] and used to evaluate the low-temperature properties of asphalt mixtures. COOPER NU-14 tester was used at test temperature of 5 °C, Poisson's ratio of 0.25, load frequency of 5 Hz, pulse rise time of 124 ms, and horizontal deformation of (5 ± 2) μm. The specimen was placed in a heat-insulated box for 5 h and then we began the test. The indirect tensile stiffness modulus is calculated according to Equation (1):

$$S_m = \frac{F(\mu + 0.27)}{zh} \times 100\%, \tag{1}$$

where S_m is the stiffness modulus, F is the median load, z is the horizontal deformation of the specimen, h is the vertical deformation of the specimen, and μ is the Poisson's ratio.

2.4.4. Splitting Test

The splitting test was carried out according to the specification JTG E20-2011 [46]. And the splitting tensile strength at 20 °C was used as the evaluation index. The loading rate was 50 mm/min. The load were recorded by computer; the splitting strength can be calculated by Equation (2). The specimens after freeze-thaw were placed in 20 °C water for 2 h and then measured the splitting tensile strength. The freeze-thaw splitting strength ratio is used as the evaluation index for water stability evaluation in specification. Therefore, the variation of the splitting tensile strength before and after freeze-thaw could be used to characterize the degradation of water stability under freeze-thaw cycles.

$$R_T = 0.006287 P_T / h, \tag{2}$$

where R_T is the splitting strength, in MPa; and h is the height of specimen, in mm.

2.4.5. Uniaxial Compression Static and Dynamic Creep Test

Uniaxial compression creep test could be used to evaluate the high-temperature performance of asphalt mixtures. The uniaxial compression static creep test was conducted by COOPER NU-14. The testing equipment is shown in Figure 5. The static creep test load was 150 kPa, the test temperature was 50 °C, the loading time was 3600 s, the preloading time was 30 s, and the pre-stress was 10 kPa. In order to ensure the uniform temperature, the specimens were placed in heat insulated box for more than 5 h before test. The square wave load was adopted for dynamic creep test. The intermittent loading (loading for 1 s and stopping for 1 s) was used. The load stress was 150 kPa, loading time was 1800 s (900 cycles), test temperature was 50 °C, and a 10 kPa preloading of 30 s was performed before the test.

Figure 5. NU-14 pneumatic servo asphalt mixture testing machine.

The creep rate is used as the evaluation index for creep test. The creep rate is the strain increase per unit time under unit stress during the stable period of deformation constant growth. The creep rate is related to the deformation rate of creep curve, which characterizes deformation resistance of asphalt mixture. The creep rate can be calculated by Equation (3):

$$\varepsilon_v = \frac{\varepsilon_2 - \varepsilon_1}{t_2 - t_1}, \tag{3}$$

where σ_0 is the creep compression stress (MPa); t_1 and t_2 are the time of the starting point and ending point of the straight line segment during the creep stabilization period, respectively; ε_1 and ε_2 are the creep strains at time t_1 and t_2, respectively; and ε_v is creep rate.

2.5. Freeze-Thaw Damage Evaluation Index

In order to evaluate the freeze-thaw resistance of asphalt mixture, the loss ratio caused by freeze-thaw damage was defined according to damage mechanics and used. The loss ratio caused by freeze-thaw damage could be defined by Equation (4):

$$D_i = \frac{E_0 - E_i}{E_0} \times 100\%, \tag{4}$$

where E_i is the performance index after i freeze-thaw cycles; and E_0 is the performance index of 0 freeze-thaw cycle.

3. Effects of Freeze-Thaw Cycles on Degradation of Performance

3.1. Mesoscopic Voidage

Binarization was used to treat the CT image. A CT scanning section of AM was taken as an example to characterize the mesoscopic voidage change under freeze-thaw cycles, as shown in Figure 6. The image processing technique and statistics were used to calculate the porosity of each layer of AM and NBAM group asphalt mixture after different freeze-thaw cycles. Image J was used as the software for image processing. The process can be divided into the following steps: (1) preset and pre-processed of CT scanner; (2) image enhancement; (3) image denoising; (4) threshold cutting and binarization of images; (5) porosity and pore morphology calculation. The relationship between mesoscopic voidage and freeze-thaw cycles was shown in Figure 7. Based on Figures 6 and 7, it can be seen that the variation law of the mesoscopic voidage is consistent with macro voidage reported in existing research. The voidage gradually increased with the increase of freeze-thaw cycles. With increasing freeze-thaw cycles, new small voidages were continuously generated and connected. At the early stage of freeze-thaw cycles (i.e., five freeze-thaw cycles), the voidage increased obviously, and then the increase tended to be stable. The voidages of AM and NBAM increased rapidly in the early stage of freeze-thaw cycles, and became stable in the middle and late state of freeze-thaw cycles.
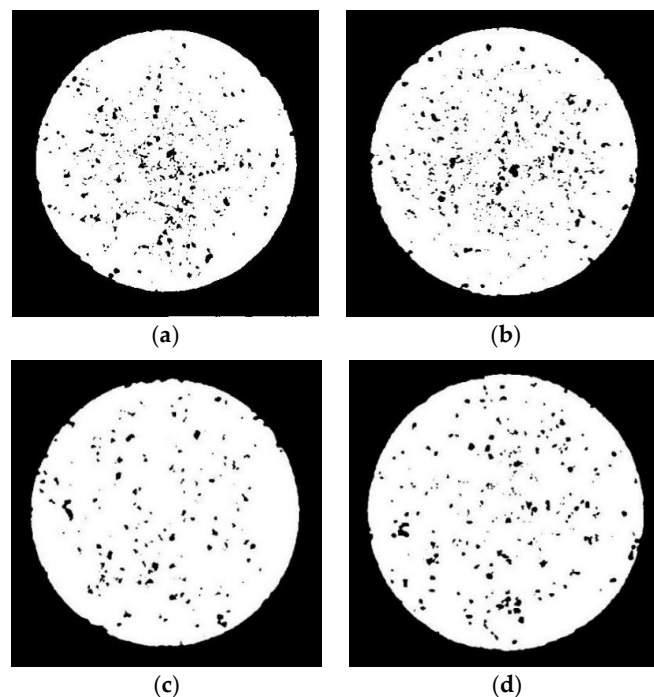

Figure 6. CT scan of sections: (**a**) 0 cycles of AM; (**b**) after five cycles of AM; (**c**) 0 cycles of NBAM; (**d**) five cycles of NBAM.
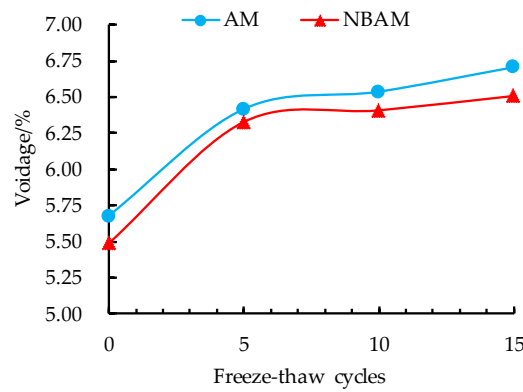
Figure 7. Variation of porosity of asphalt mixtures under freeze-thaw cycles.

3.2. Stability

The Marshall stability tests were carried out after 0, 5, 10, 15, and 20 freeze-thaw cycles. The test results are shown in Figure 8.
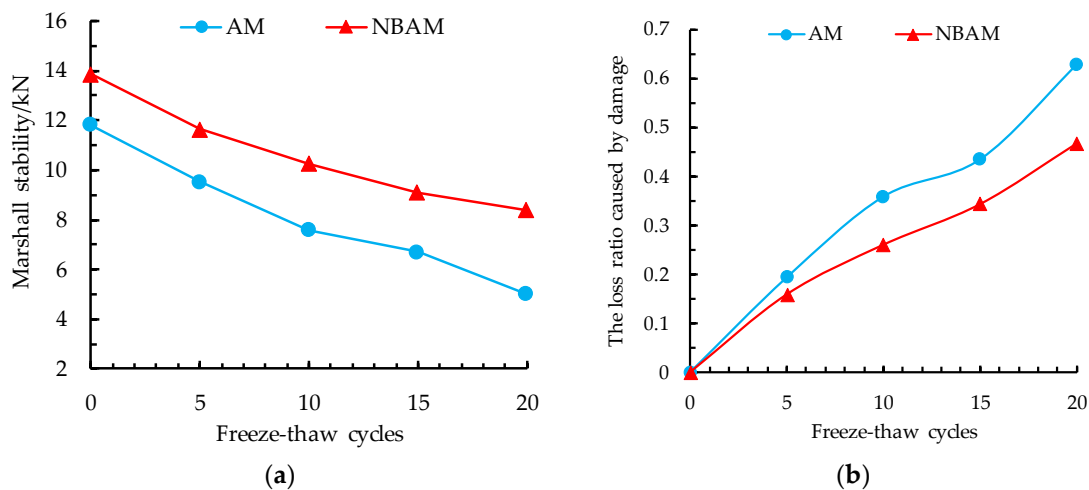

Figure 8. Stability changes: (**a**) Relationship between stability and freeze-thaw cycles; (**b**) relationship between stability damage and freeze-thaw cycles.

From Figure 8, it can be seen that the stability strength of each type of asphalt mixture was continuously reduced and the loss ratio caused by damage was continuously increased under freeze-thaw cycles. The stiffness modulus decreased slightly at the early stage of freeze-thaw cycles. After 10 freeze-thaw cycles, the performance degradation rate decreased slightly, but the loss ratio caused by damage development was relatively uniform generally. After 20 freeze-thaw cycles, the loss ratio caused by damage of NBAM group was significantly smaller than AM group. The loss ratio of stability for AM caused by damage under 20 freeze-thaw cycles is 63%, and for NBAM is 46%. The high-temperature performance of AM decreased more significantly under freeze-thaw cycles, when added nano-TiO_2/$CaCO_3$ and basalt fiber, the stability was obviously improved, and the stability loss rate was significantly reduced. The NBAM behaved an initial stability improvement of 17% over AM and NBAM increased the stability of 67% than the AM after 20 freeze-thaw cycles. The freeze-thaw resistance of NBAM was significantly better than that of AM.

From the results of mesoscopic voidage in Figure 8, as far as the whole trend was concerned, the voidage gradually increased and it increased faster at the early stage of freeze-thaw cycles. The stability gradually decreased and it decreased faster at the early stage of freeze-thaw cycles. The variation of pores was obviously related to the decline of pavement performance. Asphalt mixture freeze-thaw damage could be divided into two stages:

1. In the initial stages of freeze-thaw cycles (i.e., 0–5 cycles), the voidage increased gradually. This is because open pore water froze and expanded, which resulted in cracks in asphalt mixture. With the increase of freeze-thaw cycles, the mesoscopic cracks gradually expanded and changed into macro cracks, the voidage increased rapidly. At this stage, due to the internal cracks in asphalt mixture, the strength of asphalt mixture decreased rapidly, but the decline degree was more related to asphalt mixture types. Since the integrity of the structure was mainly provided by the bonding of the binder between aggregates, the strength of asphalt mixture decreased rapidly in the first stage after asphalt mixture cracked at the mesoscopic level. The reduction at this stage has a great relationship with asphalt mixture types. After adding nano-TiO_2/$CaCO_3$, the viscosity of the asphalt binder increased, which slowed down the cracking under the force bring by the expansion of water when it freezes. When basalt fiber was added, basalt fiber was disordered in asphalt mixture. When the crack direction was perpendicular or oblique to the fiber direction, basalt fiber played as anchor, which was similar to the reinforcement that steel provided for concrete, preventing further expansion of the crack. The uniaxial static and dynamic creep results showed that the high-temperature stability of nano-TiO_2/$CaCO_3$ and basalt fiber composite modified asphalt mixtures after freeze-thaw was significantly improved compared with other test groups.

2. In the second stage of freeze-thaw cycles (i.e., 5–15 cycles), the internal pores gradually became connected when the opening voidage increased to a certain degree, which made it possible to effectively disperse part of the frost heaving force during the freezing process. Therefore, the opening pore growth slowed down and the volume change caused by water decreased. At this stage, the water gradually began to erode the interface between asphalt and aggregate. The strength of asphalt mixture also decayed due to the loss of internal cohesive force and the moisture began to invade into the asphalt film. The stabilization phase would not continue for a long time. When the asphalt film became thinner and gradually spalled, the specimen showed significant performance degradation. The reduction trend of second stage had a greater relationship with asphalt mixture types. After the addition of nano-TiO_2/$CaCO_3$, the viscosity of asphalt binder increased and the water was more difficult to be intruded into the asphalt film, which resulted in the longer second stage. The NBAM exerted the improvement of nano-TiO_2/$CaCO_3$ completely.

In conclusion, freeze-thaw cycles reduced the high-temperature stability of asphalt mixture. When the modified material was added, the sensitivity of high-temperature stability to freeze-thaw cycles was reduced.

3.3. Dynamic Indirect Tensile Stiffness Modulus

The relationship between dynamic indirect tensile stiffness modulus and freeze-thaw cycles was shown in Figure 9. Figure 9 indicates that the dynamic indirect tensile stiffness modulus of asphalt mixture was continuously reduced and the loss ratio caused by damage was continuously increased under freeze-thaw cycles. The stiffness modulus decreased rapidly in the early stage of freeze-thaw cycles, and the performance degradation rate slowed down after 10 freeze-thaw cycles. After 20 freeze-thaw cycles, the NBAM group was significantly better than AM group. The loss ratio of stiffness modulus for AM caused by damage under 20 freeze-thaw cycles is 53%, and for NBAM is 45%. The low-temperature crack resistance of AM group was significantly reduced under freeze-thaw cycles. The stiffness modulus of NBAM group was 20% higher than AM group. The stiffness modulus of NBAM group increased by 41% compared to AM group after 20 freeze-thaw cycles. The freeze-thaw resistance of NBAM group was obviously better than AM group. The freeze-thaw cycles reduced the low-temperature indirect tensile stiffness modulus of asphalt mixtures. The addition of nano-TiO_2/$CaCO_3$ and basalt fiber reduced the sensitivity of the low-temperature crack resistance to freeze-thaw cycles.
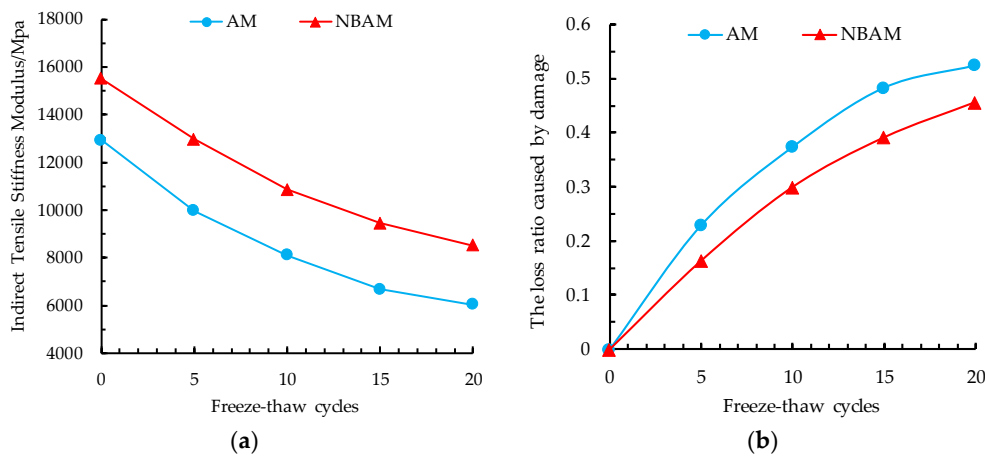
Figure 9. Relationship between indirect tensile stiffness modulus and freeze-thaw cycles: (**a**) indirect tensile stiffness modulus; (**b**) loss ratio of stiffness modulus caused by damage.

3.4. Splitting Tensile Strength

After 0, 5, 10, 15, and 20 freeze-thaw cycles, splitting tests were carried out. The test results are shown in Figure 10.
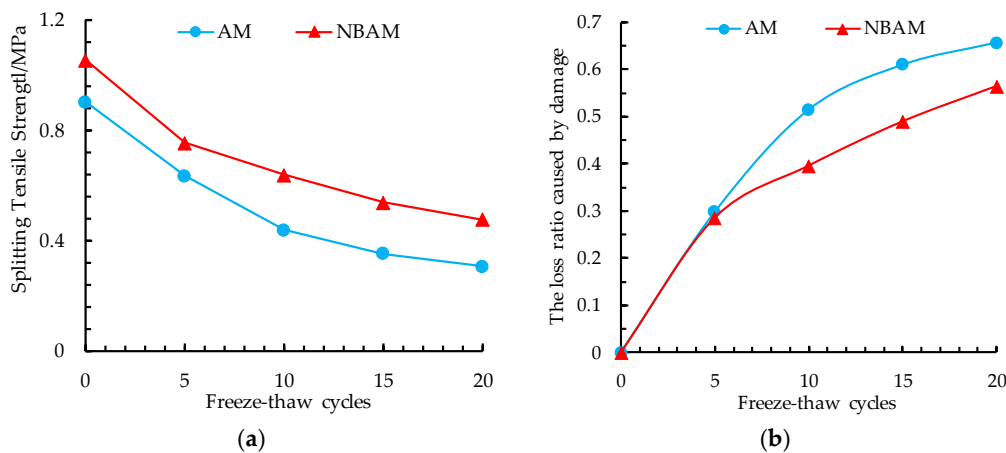

Figure 10. Relationship between splitting tensile strength and freeze-thaw cycles: (**a**) splitting tensile strength trend chart; (**b**) loss ratio of splitting tensile strength caused by damage.

It can be seen from Figure 10 that the splitting tensile strength of asphalt mixture reduced and the loss ratio caused by damage increased continuously under freeze-thaw cycles. In the early stage of freeze-thaw cycle, the splitting tensile strength reduced rapidly. The performance degradation rate was gradually slowed down after 10 freeze-thaw cycles. When the freeze-thaw cycles of 20, the loss ratio caused by damage of NBAM group was significantly smaller than that of AM group. The loss ratio of splitting tensile strength for AM caused by damage under 20 freeze-thaw cycles is 67%, and for NBAM is 56%. The water stability of asphalt mixture matrix was decreased more significantly under freeze-thaw cycles. When nano-TiO_2/$CaCO_3$ and basalt fiber were added, the splitting tensile strength increased and the stability loss rate decreased significantly. It indicated that the addition of nano-TiO_2/$CaCO_3$ and basalt fiber could jointly exert the improvements of two materials on water stability. The splitting tensile strength of NBAM group was 16% higher than AM group under 0 freeze-thaw cycles. After 20 freeze-thaw cycles, the splitting tensile strength of NBAM group increased 48% compared to AM group. The freeze-thaw resistance of NBAM group was obviously better than that of AM group. The freeze-thaw cycles reduced the splitting tensile strength of asphalt mixture.

When nano-TiO_2/$CaCO_3$ and basalt fiber were added, the sensitivity of water stability to freeze-thaw cycles was reduced.

3.5. Static and Dynamic Compression Creep

Considering the creep test was greatly affected by the preparation of the specimen, the influence of preparation would mask the actual influence of freeze-thaw cycles on high-temperature creep characteristics when the interval between freeze-thaw cycles was short. Therefore, asphalt mixture specimens after 0 and 15 freeze-thaw cycles were used for comparative analysis. The creep curves of asphalt mixtures before and after freeze-thaw cycles were shown in Figures 11 and 12.
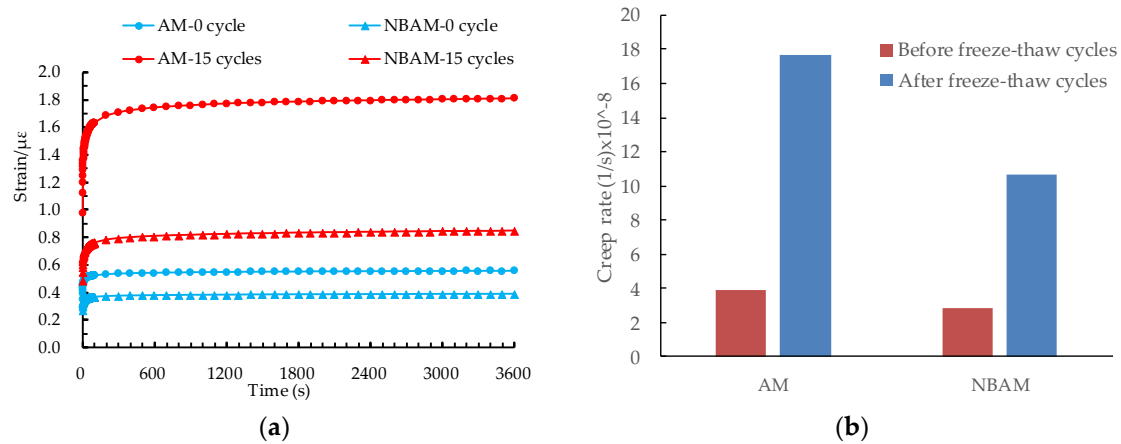
Figure 11. Static creep: (**a**) relationship between static creep time and strain; (**b**) the change of creep rate.
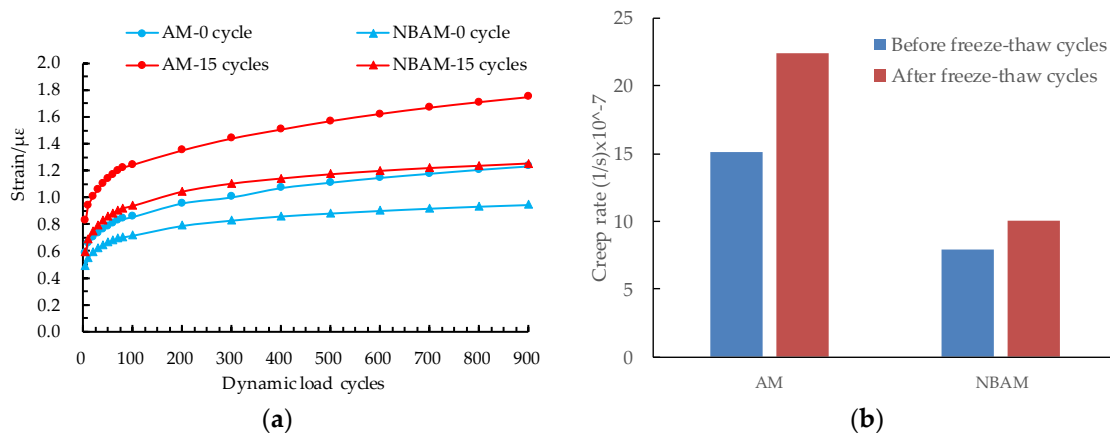

Figure 12. Dynamic creep: (**a**) relationship between dynamic creep time and strain; (**b**) the change of creep rate.

Figures 11a and 12a indicate that the creep curve could be clearly divided into two stages: (1) Migration period: creep deformation increased rapidly at the moment of loading and the creep rate decreased rapidly as time went on. (2) Stable period: the creep deformation increased linearly and the creep rate remained constant. In Figure 11a, the curve entered stable period after 1000 s, so t_1 and t_2 could be taken as 1000 s and 3600 s to calculate the creep rate in the stable period. In Figure 12a, the curve entered stable period after 500 cycles (1000 s), so it was possible to calculate the creep rate by taking t_1 = 1000 s and t_2 = 1800 s. Comparing the creep curves before and after freeze-thaw cycles, it could be concluded that the total strain of two types of asphalt mixtures increased under freeze-thaw cycles, after 15 freeze-thaw cycles, the curve of creep time and strain moved up significantly, which fully demonstrated that the freeze-thaw cycles occurred damage of specimens. The creep strain of NBAM group was smaller than that of AM group and the strain difference between the two groups after

freeze-thaw cycles was smaller, which indicated that the deformation resistance at high temperature was enhanced and the modifiers reduced the sensitivity of high-temperature performance to the freeze-thaw cycles. Comparing the creep rate change before and after freeze-thaw cycles, the static creep rate of each type of asphalt mixture increased significantly. The AM group increased 3-fold, while the NBAM group doubled. The dynamic creep rate also increased after freeze-thaw cycles. The creep rate was negatively correlated with the dynamic stability. Therefore, it could be concluded that the anti-rutting ability of asphalt mixture was significantly reduced after freeze-thaw cycles. The degradation trend was obviously weakened when the modified materials were added. In summary, the freeze-thaw cycles reduced the high-temperature stability of asphalt mixture, and at the same time, the addition of nano-TiO_2/$CaCO_3$ and basalt fiber reduced the sensitivity of high-temperature stability to the freeze-thaw cycles.

The stability, stiffness modulus, and splitting tensile strength of the NBAM group were 17%, 20%, and 16% higher than those of the AM group before the freeze-thaw cycle. After 20 freeze-thaw cycles, these indexes were 67%, 41%, and 48% higher than AM group, respectively. It can be seen that the basalt fiber and nano-TiO_2/$CaCO_3$ can effectively improve the performance of asphalt mixture under freeze-thaw cycles. From the performance of NBAM and AM after 15 F–T cycles, we can conclude that the DBFAM pavement can present longer service life in seasonal frozen regions. This is important for reducing road maintenance and traffic disruption, and the costs expected for AM and NBAM are 0.330 CNY/Kg and 0.403 CNY/Kg. It is still important in seasonal frozen regions of China, although the cost of the modified asphalt mixture has increased.

4. Analysis of Damage Model of Asphalt Mixture Based on Grey Theory

The existed methods for damage prediction model of asphalt mixture after the freeze-thaw cycles mainly included: BP neural network method, support vector machine method, probability statistics and grey theory. The gray theory GM (1, N) model was a widely used prediction model [51–53]. It required less useful information and had higher prediction accuracy. In this study, the interaction between various properties of asphalt mixture and freeze-thaw damage was considered. The equal-pitch gray prediction model GM (1, 3) was used to predict the freeze-thaw damage of asphalt mixture.

The establishment of the GM (1, N) model is described in the literature [51], and the final results are shown in Equations (5) and (6):

$$\hat{x}_1^{(1)}(k+1) = \left[x_1^{(0)}(1) - \frac{1}{\hat{\alpha}} \sum_{i=2}^{n} \hat{b}_{i-1} x_1^{(1)}(k-1) \right] e^{-\alpha k} + \frac{1}{\hat{\alpha}} \sum_{i=2}^{n} \hat{b}_{i-1} x_i^{(1)}(k+1), k = 1, 2, \ldots, n, \quad (5)$$

$$\hat{x}_1^{(0)}(k+1) = \hat{x}_1^{(1)}(k+1) - \hat{x}_1^{(1)}(k), k = 1, 2, \ldots, n. \quad (6)$$

In this study, GM (1, 3) prediction model was established with matlab program according to the reference [51]. The freeze-thaw data were fitted respectively, the stability, splitting tensile strength damage and stiffness modulus damage of asphalt mixture after freeze-thaw damage were taken as $X_1^{(0)}$ sequence, $X_2^{(0)}$ sequence and $X_3^{(0)}$ sequence. The asphalt mixture specimens were tested and the prediction model was established after 0, 5, 10, 15 freeze-thaw cycles. The prediction was conducted based on 20 times GM (1, 3) model. Because the grey theory model conducted iterative prediction based on the previous data, this study selected the 15th measured data for derivation. The 20th prediction results were compared with actual data and the prediction accuracy was analyzed. Prediction damage and error are shown in Table 7.

Table 7. Twentieth cycle prediction data of asphalt mixture.

Performances		AM	NBAM
Stability	Predictive value (kN)	5.02	8.40
	Measured value (kN)	4.40	7.38
	Absolute error (%)	12.4	12.1
Indirect tensile stiffness modulus	Predictive value (MPa)	6023.7	8523.0
	Measured value (MPa)	6144.2	8426.9
	Absolute error (%)	2.0	1.1
Splitting tensile strength	Predictive value (MPa)	0.31	0.48
	Measured value (MPa)	0.31	0.46
	Absolute error (%)	0.5	4.0

Table 7 indicated that the relative errors between the calculated results and experimental results were less than 15%. Comparing the predicted results of GM (1, 3) model for each performance index, it can be concluded that the predicted results of splitting tensile strength were the best and its absolute values were all small. The prediction result of indirect tensile modulus was better, while the prediction result of stability had a certain error. However, all were less than 15%. Therefore, the established GM (1, 3) gray prediction model could better predict the stability, indirect tensile stiffness modulus and splitting tensile strength of asphalt mixture under freeze-thaw cycles.

The prediction curves of the loss ratio caused by freeze-thaw damage of stability, splitting tensile strength and stiffness modulus of four asphalt mixtures with GM (1, 3) model are shown in Figure 13.
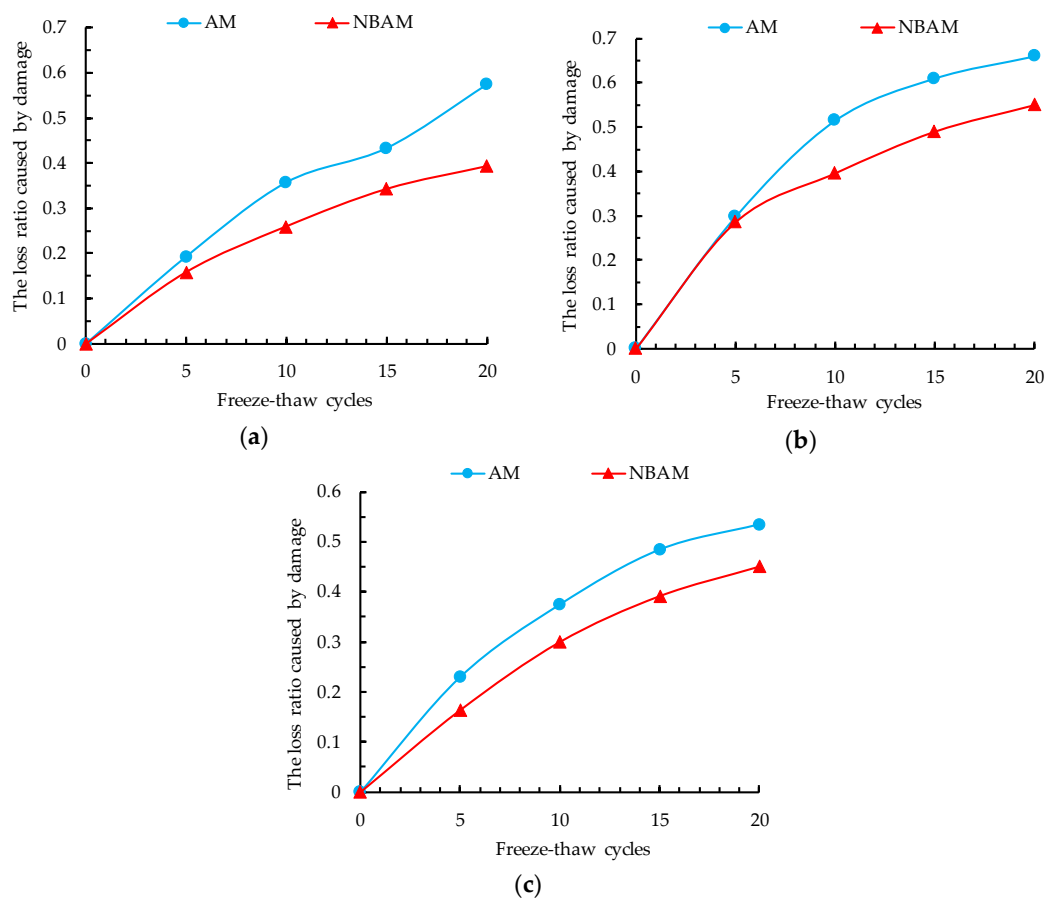

Figure 13. Prediction curves of loss ratio caused by damage: (**a**) loss ratio caused by damage of stability prediction curve; (**b**) loss ratio caused by damage of splitting strength prediction curve; (**c**) loss ratio caused by damage of stiffness modulus prediction curve.

5. Conclusions

This study studied the pavement performance degradation laws of nano-TiO_2/$CaCO_3$ and basalt fiber composite modified asphalt mixtures under freeze-thaw cycles. The improvement of modifiers on freeze-thaw resistance of asphalt mixture was studied by measuring mesoscopic voidage, stability, indirect tensile stiffness modulus, splitting strength, and uniaxial compression static and dynamic creep rate. The GM (1, 3) model was established to predict the pavement performance of the modified asphalt mixture. The following conclusions were obtained:

- With the increasing freeze-thaw cycles, the mesoscopic void ratio of asphalt mixture increased, the stability, splitting tensile strength and indirect tensile stiffness modulus decreased. The properties of nano-TiO_2/$CaCO_3$ and basalt fiber composite modified asphalt mixtures were better than other test groups before and after freeze-thaw cycles. Before freeze-thaw cycle, the stability, stiffness modulus and splitting tensile strength of NBAM group were 17%, 20% and 16% higher than those of AM group, and they are 67%, 41%, and 48% after 20 freeze-thaw cycles.

- The uniaxial static and dynamic creep results showed that the high-temperature stability of nano-TiO_2/$CaCO_3$ and basalt fiber composite modified asphalt mixtures after freeze-thaw was significantly improved compared with other test groups. Comparing the creep rate change before and after freeze-thaw cycles, the static creep rate of each type of asphalt mixture increased significantly. AM group increased by three times, while NBAM group increased by two times. The dynamic creep rate also increased after freeze-thaw cycles. The creep rate was negatively correlated with the dynamic stability.

- The GM (1, 3) model was used to predict various properties of modified asphalt mixture and the prediction results with high accurate were obtained. It indicated that GM (1, 3) model was suitable to predict the stability, indirect tensile stiffness modulus, and splitting tensile strength of the asphalt mixture under freeze-thaw cycles.

References

1. Kogbara, R.B.; Masad, E.A.; Kassem, E.; Scarpas, A.; Anupam, K. A state-of-the-art review of parameters influencing measurement and modeling of skid resistance of asphalt pavements. *Constr. Build. Mater.* **2016**, *114*, 602–617. [CrossRef]

2. Si, W.; Li, N.; Ma, B.; Ren, J.P.; Wang, H.N.; Hu, J. Impact of freeze-thaw cycles on compressive characteristics of asphalt mixture in cold regions. *J. Wuhan Univ. Technol. (Mater. Sci. Ed.)* **2015**, *4*, 703–709. [CrossRef]

3. Ameri, M.; Kouchaki, S.; Roshani, H. Laboratory evaluation of the effect of nano-organosilane anti-stripping additive on the moisture susceptibility of HMA mixtures under freeze–thaw cycles. *Constr. Build. Mater.* **2013**, *48*, 1009–1016. [CrossRef]

4. Hamedi, G.H.; Nejad, F.M.; Oveisi, K. Investigating the effects of using nanomaterials on moisture damage of HMA. *Road Mater. Pavement* **2015**, *16*, 536–552. [CrossRef]

5. Shafabakhsh, G.H.; Ani, O.J. Experimental investigation of effect of Nano TiO_2/SiO_2 modified bitumen on the rutting and fatigue performance of asphalt mixtures containing steel slag aggregates. *Constr. Build. Mater.* **2015**, *98*, 692–702. [CrossRef]

6.   Mostafa, S.; Gholamali, S. Use of Nano SiO$_2$ and Nano TiO$_2$ to improve the mechanical behaviour of stone mastic asphalt mixtures. *Constr. Build. Mater.* **2017**, *157*, 965–974.

7.   Nazari, H.; Naderi, K.; Nejad, F.M. Improving aging resistance and fatigue performance of asphalt binders using inorganic nanoparticles. *Constr. Build. Mater.* **2018**, *170*, 591–602. [CrossRef]

8.   Zheng, Y.X.; Cai, Y.C.; Zhang, Y.M. Laboratory study of pavement performance of basalt fiber-modified asphalt mixture. *Adv. Mater. Res.* **2011**, *266*, 175–179. [CrossRef]

9.   Fan, W.X.; Kang, H.G.; Zheng, Y.X. Experimental study of pavement performance of basalt fiber modified asphalt mixture. *J. Southeast Univ. (Engl. Ed.)* **2010**, *26*, 614–617.

10.   Morova, N. Investigation of usability of basalt fibers in hot mix asphalt concrete. *Constr. Build. Mater.* **2013**, *47*, 175–180. [CrossRef]

11.   Chen, Y.Z.; Li, Z.X. Study of Road Property of Basalt Fiber Asphalt Concrete. *Appl. Mech. Mater.* **2012**, *238*, 22–25. [CrossRef]

12.   Qin, X.; Shen, A.Q.; Guo, Y.C.; Li, Z.N.; Lv, Z.H. Characterization of asphalt mastics reinforced with basalt fibers. *Constr. Build. Mater.* **2018**, *159*, 508–516. [CrossRef]

13.   Gao, C.M.; Dong, W.Z.; Liu, X.Y.; Wang, H.; Zhang, M.L. Tensional ability of basalt fiber enforced asphalt mixture. *Appl. Mech. Mater.* **2011**, *97*, 837–840. [CrossRef]

14.   Chang, R.; Hao, P.W. Impact of freeze-thaw cycles with salt on low temperature properties of asphalt mixture. *J. Build. Mater.* **2017**, *20*, 481–488.

15.   Davar, A.; Tanzadeh, J.; Fadaee, O. Experimental evaluation of the basalt fibers and diatomite powder compound on enhanced fatigue life and tensile strength of hot mix asphalt at low temperatures. *Constr. Build. Mater.* **2017**, *153*, 238–246. [CrossRef]

16.   Zheng, Y.X.; Cai, Y.C.; Zhang, G.H.; Fang, H.Y. Fatigue property of basalt fiber-modified asphalt mixture under complicated environment. *J. Wuhan Univ. Technol. (Mater. Sci. Ed.)* **2014**, *29*, 996–1004. [CrossRef]

17.   Zhang, K.; Zhang, Z.Q. Deterioration of mechanical properties of asphalt mixture in salty and humid environment. *J. S. China Univ. Technol. (Nat. Sci. Ed.)* **2015**, *43*, 106–112.

18.   Zhang, Z.Q.; Zhang, K. Influence of additives on the water stability of asphalt mixture in salty and humid environment. *J. Funct. Mater.* **2015**, *46*, 21128–21132.

19.   Celauro, C.; Pratico, F.G. Asphalt mixtures modified with basalt fibers for surface courses. *Constr. Build. Mater.* **2018**, *170*, 245–253. [CrossRef]

20.   Ni, P. Study on Design and Pavement Performance Experiment of Basalt Fiber SMA-13 Mixture. Master's Thesis, Jilin University, Changchun, China, 2017.

21.   Mu, Y. Research of Reinforced Basalt Fiber Applied in Asphalt Pavement with Heavy Traffic. Master's Thesis, Chang'an University, Xi'an, China, 2016.

22.   Zhao, L.D. Influencing Factors and Meso Mechanism of Asphalt Pavement Damages Caused by Condensate Ice. Ph.D. Thesis, Harbin Institute of Technology University, Harbin, China, 2012.

23.   Cheng, Y.C.; Di, Y.; Tan, G.J.; Zhu, C.F. Low-temperature performance and damage constitutive model of Eco-friendly basalt fiber–diatomite-modified asphalt mixture under freeze-thaw cycles. *Materials* **2018**, *11*, 2148. [CrossRef]

24.   Cheng, Y.C.; Di, Y.; Gong, Y.F.; Zhu, C.F.; Tao, J.L.; Wang, W.S. Laboratory evaluation on performance of Eco-friendly basalt fiber and diatomite compound modified asphalt mixture. *Materials* **2018**, *11*, 2400. [CrossRef]

25.   Bi, H.P. Research on Performance and Microscopic Properties of Asphalt Mixture Modified by Nano 505 TiO$_2$/CaCO$_3$ and Basalt Fiber. Ph.D. Thesis, Jilin University, Changchun, China, 2018.

26.   Xu, H.N.; Li, H.Z.; Tan, Y.Q.; Wang, L.B.; Hou, Y.A. Micro-scale investigation on the behaviors of asphalt mixtures under freeze-thaw cycles using entropy theory and a computerized tomography scanning technique. *Entropy* **2018**, *20*, 68–79. [CrossRef]

27.   Nian, T.F.; Li, P.; Mao, Y.; Zhang, G.H.; Liu, Y. Connections between chemical composition and rheology of aged base asphalt binders during repeated freeze-thaw cycles. *Constr. Build. Mater.* **2018**, *159*, 338–350. [CrossRef]

28. Xu, H.; Guo, W.; Tan, Y. Internal structure evolution of asphalt mixtures during freeze-thaw cycles. *Mater. Des.* **2015**, *86*, 436–446. [CrossRef]

29. Xu, H.; Wei, G.; Tan, Y. Permeability of asphalt mixtures exposed to freeze–thaw cycles. *Cold Reg. Sci. Technol.* **2016**, *123*, 99–106. [CrossRef]

30. Wang, Y.Q.; Tan, Y.Q.; Guo, M.; Wang, X.L. Effect of freeze-thaw cycles on the internal structure and performance of semirigid base materials. *Adv. Mater. Sci. Eng.* **2017**, *2017*. [CrossRef]

31. Ma, B.; Si, W.; Zhu, D.P.; Wang, H.N. Applying method of moments to model the reliability of deteriorating performance to asphalt pavement under freeze-thaw cycles in cold regions. *J. Mater. Civ. Eng.* **2015**, *27*, 04014103. [CrossRef]

32. Lachance-Tremblay, E.; Perraton, D.; Vaillancourt, M.; Di-Benedetto, H. Degradation of asphalt mixtures with glass aggregates subjected to freeze-thaw cycles. *Cold Reg. Sci. Technol.* **2017**, *141*, 8–15. [CrossRef]

33. Badeli, S.; Carter, A.; Dore, G. Complex modulus and fatigue analysis of an asphalt mix after daily rapid freeze-thaw cycles. *J. Mater. Civ. Eng.* **2018**, *30*, 04018056. [CrossRef]

34. Badeli, S.; Carter, A.; Dore, G. Effect of laboratory compaction on the viscoelastic characteristics of an asphalt mix before and after rapid freeze-thaw cycles. *Cold Reg. Sci. Technol.* **2018**, *146*, 98–109. [CrossRef]

35. Badeli, S.; Carter, A.; Dore, G.; Saliani, S. Evaluation of the durability and the performance of an asphalt mix involving Aramid Pulp Fiber (APF): Complex modulus before and after freeze-thaw cycles, fatigue, and TSRST tests. *Constr. Build. Mater.* **2018**, *174*, 60–71. [CrossRef]

36. Gong, X.B.; Romero, P.; Dong, Z.J.; Sudbury, D.S. The effect of freeze–thaw cycle on the low-temperature properties of asphalt fine aggregate matrix utilizing bending beam rheometer. *Cold Reg. Sci. Technol.* **2016**, *125*, 101–107. [CrossRef]

37. Ho, C.H.; Linares, C.P.M. Representation functions to predict relaxation modulus of asphalt mixtures subject to the action of freeze-thaw cycles. *J. Transp. Eng. Part B-Pavements* **2018**, *144*, 04018013. [CrossRef]

38. Sol-Sanchez, M.; Moreno-Navarro, F.; Garcia-Trave, G.; Rubio-Gamez, M.C. Laboratory study of the long-term climatic deterioration of asphalt mixtures. *Constr. Build. Mater.* **2015**, *88*, 32–40. [CrossRef]

39. Huang, S.C.; Robertson, R.E.; Branthaver, J.F.; Petersen, J.C. Impact of lime modification of asphalt and freeze–thaw cycling on the asphalt–aggregate interaction and moisture resistance to moisture damage. *J. Mater. Civ. Eng.* **2005**, *17*, 711–718. [CrossRef]

40. Wei, H.; Li, Z.; Jiao, Y. Effects of diatomite and SBS on freeze-thaw resistance of crumb rubber modified asphalt mixture. *Adv. Mater. Sci. Eng.* **2017**, *2017*. [CrossRef]

41. Modarres, A.; Ramyar, H.; Ayar, P. Effect of cement kiln dust on the low-temperature durability and fatigue life of hot mix asphalt. *Cold Reg. Sci. Technol.* **2015**, *110*, 59–66. [CrossRef]

42. Yan, K.Z.; Ge, D.D.; You, L.Y.; Wang, X.L. Laboratory investigation of the characteristics of SMA mixtures under freeze–thaw cycles. *Cold Reg. Sci. Technol.* **2015**, *119*, 68–74. [CrossRef]

43. Xu, H.Y.; Dang, S.Y.; Cui, D.Y. Durability test research of asphalt mixture with rubber particles under the condition of freeze-thaw cycle. *Adv. Mater. Sci. Eng.* **2014**, *919–921*, 1096–1099. [CrossRef]

44. Teguedi, M.C.; Toussaint, E.; Blaysat, B.; Moreira, S.; Liandrat, S.; Grediac, M. Towards the local expansion and contraction measurement of asphalt exposed to freeze-thaw cycles. *Constr. Build. Mater.* **2017**, *154*, 438–450. [CrossRef]

45. JTG F40-2004. *Technical Specifications for Construction of Highway Asphalt Pavements*; Ministry of Transport: Beijing, China, 2004. (In Chinese)

46. JTG E20-2011. *Standard Test Methods of Asphalt and Asphalt Mixtures for Highway Engineering*; Ministry of Transport: Beijing, China, 2011. (In Chinese)

47. Yang, J.S. Study on Road Performance and Low Temperature Characteristics of Basalt Fiber SMA-13. Master's Thesis, Jilin University, Changchun, China, 2018.

48. JT/T 776.1-2010. *Basalt Fiber and Product for Highway Engineering—Part 1: Basalt Fiber Chopped Strand*; Ministry of Transport: Beijing, China, 2010. (In Chinese)

49. JTG E42-2005. *Test Methods of Aggregate for Highway Engineering*; Ministry of Transport: Beijing, China, 2005. (In Chinese)

50. EN 12697-26. Bituminous Mixtures—Test Methods for Hot Mix Asphalt—Part 26: Stiffness. British Standard Institution: London, UK, 2012.

51. Ren, J.Z.; Gao, S.Z.; Tan, S.Y.; Dong, L.C. Prediction of the yield of biohydrogen under scanty data conditions based on GM (1, N). *Int. J. Hydrogen Energy* **2013**, *38*, 13198–13203. [CrossRef]

52. Ren, J.Z. GM (1, N) method for the prediction of anaerobic digestion system and sensitivity analysis of influential factors. *Bioresour. Technol.* **2017**, *247*, 1258–1261. [CrossRef]

53. Liu, H.H.; Liu, Z.B.; Ding, X.F. A new oilfield production prediction method based on GM (1, n). *Pet. Sci. Technol.* **2014**, *32*, 22–28. [CrossRef]